Blind test comparison of the performance and wake flow between two in-line wind turbines exposed to different atmospheric inflow conditions

Jan Bartl[1], Lars Sætran[1]

[1] Department of Energy and Process Engineering, Norwegian University of Science and Technology, Trondheim, 7491, Norway

Correspondence to: Jan Bartl (jan.bartl@ntnu.no)

Abstract. This is a summary of the results of the fourth Blind test workshop which was held in Trondheim in October 2015. Herein, computational predictions on the performance of two in-line model wind turbines as well as the mean and turbulent wake flow are compared to experimental data measured at NTNU's wind tunnel. A detailed description of the model geometry, the wind tunnel boundary conditions and the test case specifications was published before the workshop. Expert groups within Computational Fluid Dynamics (CFD) were invited to submit predictions on wind turbine performance and wake flow without knowing the experimental results at the outset. The focus of this blind test comparison is to examine the model turbines' performance and wake development up until 9 rotor diameters downstream at three different atmospheric inflow conditions. Besides a spatially uniform inflow field of very low turbulence intensity (TI=0.23%) as well as high turbulence intensity (TI=10.0%), the turbines are exposed to a grid-generated atmospheric shear flow (TI=10.1%).

Five different research groups contributed with their predictions using a variety of simulation models, ranging from fully resolved Reynolds Averaged Navier Stokes (RANS) models to Large Eddy Simulations (LES). For the three inlet conditions the power and the thrust force of the upstream turbine is predicted fairly well by most models, while the predictions of the downstream turbine's performance show a significantly higher scatter. Comparing the mean velocity profiles in the wake, most models approximate the mean velocity deficit level sufficiently well. However, larger variations between the models for higher downstream positions are observed. The prediction of the turbulence kinetic energy in the wake is observed to be very challenging. Both the LES model and the IDDES (Improved Delayed Detached Eddy Simulation) model, however, are consistently managing to provide fairly accurate predictions of the wake turbulence.

1 Introduction

Given the constraints of transmission and installation costs the available area for offshore wind farm installations is fairly limited. Under these circumstances wake interactions play an important role when evaluating the energy production since the energy captured by an upstream wind turbine leaves significantly less energy in the wake for the downstream turbine. For certain wind directions these power losses are estimated to account for up to 10-20% for large offshore wind farms

(Barthelmie et al., 2009). Furthermore, the rotor generated turbulence in the wake is a source for augmented material fatigue on the downstream rotor.

In order to be able to come up with holistic control approaches for optimising a wind farm well-performing prediction tools for the wake flow behind a wind turbine rotor for all kinds of atmospheric conditions are needed. Therefore, the development

5 of simple wake models began already in the early 1980s. Analytical wake models by Jensen (1983), Ainslie (1988), Crespo et al. (1988), Frandsen et al. (2006) or Larsen et al. (2008) are based on a number of simplifications and calibrated with empirical parameters. Most of the state-of-the-art software used for industrial wind farm planning is still based on these engineering wake models. However, they are not able to reconstruct the wake characteristics to a sufficient degree of detail (Sanderse et al., 2011).

10 With an increase in computational power advanced CFD models based on more fundamental physics arose. These CFD models are computationally more expensive but are able to resolve the flow structures in much larger detail. In general, two types of CFD approaches are state of the art in wake modelling: Reynolds Averaged Navier Stokes (RANS) equations that are averaging the turbulent fluctuations as well as the computationally more expensive Large Eddy Simulations (LES) which are solving for large eddies only. Hybrid models like Detached Eddy Simulations (DES) combine the advantages of

15 calculating unsteady flow effects from LES as well as resolving small scales in the boundary layers as RANS does. Another challenge is the modelling of the interaction of the wind turbine rotor with the flow: the rotor geometry can either be fully resolved or simplified as a two-dimensional force field. The latter option is usually more efficient with respect to computational time. In RANS models it is possible to fully resolve the rotor geometry and thus model complex three-dimensional flow. In LES models, however, a full resolution of the rotor geometry is difficult as the smaller scales which

20 determine the forces at the surfaces of interaction are not resolved. Thus, the rotor is often modelled as a two-dimensional force field which requires detailed knowledge of the lift and drag forces that act under certain inflow conditions.

Even though the wake behind full-scale wind turbine has recently been measured (Kocer et al., 2011), (Kumer et al., 2015), (Trujillo et al., 2016), the disordered inflow conditions in full-scale experiments make it very difficult to use those data to verify wake prediction models. Therefore, wind tunnel experiments on model turbines under controlled boundary conditions

25 are an appropriate method to verify simulation tools.

Despite the drawbacks of low Reynolds numbers and possible wall blockage effects in model experiments a number of well-defined comparison tests have been conducted. One of the first model scale experiments was the investigation by Talmon (1985). On a small rotor of the diameter of D=0.36m the wake was measured in order to serve as a reference experiment for calculations. In addition to uniform inflow the wake development is studied in a simulated atmospheric boundary layer.

30 Another seminal investigation was conducted by Medici and Alfredsson (2006). With three-dimensional wake flow measurements on a D=0.18m model turbine down to x/D=9 they shed light on phenomena like wake rotation, wake deflection in yawed operation and bluff body vortex shedding frequencies from the rotor.

At the Norwegian University of Science and Technology (NTNU) two model turbines of the rotor diameter D=0.90m were extensively investigated. Adaramola and Krogstad (2011) were analysing the effect of modifying tip speed ratio, blade pitch

angle and yaw angle on a downstream turbine. Eriksen (2016) investigated the three dimensional rotor generated turbulence in the wake of one model turbine in detail. Bartl et al. (2012) were examining the wake behind two model turbines, while special attention to asymmetries and wake rotation was given by Schümann et al. (2013). A recent study by Bartl and Sætran (2016) investigated the interrelation of wake flow and the performance of a downstream turbine for axial-induction based wind farm control methods.

The largest rotor investigated for wake comparison studies was the MEXICO rotor with a diameter of 4.5m (Schepers et al., 2010), in which the rotor performance as well as the wake flow are examined in detail. A second campaign investigating even more effects including spanwise pressure distributions, yaw misalignment and unsteady effects was realized at the large German Dutch Wind Tunnel (DNW). A benchmark comparison of the comprehensive set of measurement data with numerical calculations is found in Schepers et al. (2014).

In 2011 the first Blind test work shop on turbine performance and wake development behind one model turbine was organized. The geometry of the model turbine and wind tunnel environment was made available to the public and dedicated research groups were invited to predict the model turbine's performance and the wake development up to x/D = 5.0 rotor diameters downstream. A total of 11 sets of predictions were submitted and reported by Krogstad and Eriksen (2013). This first Blind test experiment showed a significant scatter in the performance predictions with a variation of several magnitudes in predictions of turbulent quantities in the wake between the different contributions. Therefore, it was decided to perform another Blind test workshop in 2012 increasing the test complexity by adding a second turbine aligned with the upstream turbine. The participants were asked to predict the performance of both turbines as well as the wake behind the downstream turbine. Nine different submissions were received showing clear variations in the quality of the predictions between the different modelling methods (Pierella et al., 2014). For a third blind test workshop held in 2013 the complexity was slightly increased again. The two model wind turbines were positioned with a span-wise offset of half a rotor diameter. The results reported by Krogstad et al. (2014) showed that a LES simulation method proved to simulate this complex flow case fairly well.

2 Methods

2.1 Test case description

2.1.1 Wind tunnel

The experimental data of this study are measured in the closed-loop wind tunnel at NTNU in Trondheim. The rectangular test section of the wind tunnel is 2.71 m broad, 1.81 m high and 11.15 m long. The wind tunnel roof is adjusted for a zero pressure gradient generating a constant velocity in the entire test section. The wind tunnel inlet speed is controlled by an inlet contraction which is equipped with static pressure holes at the circumferences at two defined cross sections. Figure 1 shows a picture of the test section with the two model turbines installed at a streamwise separation distance of $x/D_{T2}=2.77$.

The wind tunnel is driven by a 220kW fan located downstream of the test section being able to generate maximum wind speeds of up to U_{max}=30m/s.

2.1.2 Model turbines, rotor and airfoil characteristics

5   The model wind turbines have a three-bladed rotor with a diameter of D_{T1}=0.944m and D_{T2}=0.894m. The small difference in rotor diameter stems from a slightly different hub geometry of the rigs. Apart from that the blade geometry is exactly the same. Both turbines rotate in the counter-clockwise direction when observed from an upstream point of view. The rotors are both driven by a 0.37 kW AC Siemens electric motor and controlled by a Siemens Micromaster 440 frequency inverter. The motor rotational speed can be varied from about 100 – 3000 rpm while the generated power is burned off by an external load

10   resistance.

The turbine blades were designed using the NREL S826 airfoil from the root to the tip. The airfoil, as shown in Fig. 2, was designed at the National Renewable Energy Laboratory (NREL) and a detailed description of the airfoil's characteristics is given by Somers (2005). Herein, the geometry is specified and the performance characteristics estimated. Lift and drag coefficients are presented for a range of operating Reynolds numbers ($Re_{C,tip,FS}$=10^6) for a full scale turbine, which are one

15   order of magnitude higher than the Reynolds numbers prevailing in this model experiment ($Re_{C,tip,model}$=10^5). In order to be able to characterise the airfoil's performance also at model scale Reynolds numbers, a number of 2D experiments on airfoil performance have been conducted. Sarmast and Mikkelsen (2013) performed an experiment on a two dimensional S826 wing section of the chord length c_L=0.10m at DTU in Denmark. They observed hysteretic behaviour for $Re_c < 10^5$ which is assumed to be the cause for Reynolds-dependent behaviour of the inner blade elements of the upstream turbine under design

20   conditions. Another experimental set of S826 airfoil data is presented by Ostovan et al. (2013) from METU in Turkey. They investigated lift and drag coefficients from Re_C=$7.15 \cdot 10^4$ to Re_C=$1.45 \cdot 10^5$ on a 2D wing with a chord length of c_L=0.20m. No hysteretic effects for low Reynolds numbers are found in this experiment. A third experimental set of airfoil characteristics from Re_C=$7.00 \cdot 10^4$ to Re_C=$6.00 \cdot 10^5$ has been measured by Aksnes (2015) on a wing section of c_L=0.45m at NTNU, Norway. Neither in this experiment is any Reynolds-dependent behaviour at low Reynolds numbers found. The measured lift and drag

25   coefficients of these three experiments are in good agreement in the linear lift region, while in the pre-stall and stall region significant differences between the three datasets are present. For Re_C=10^5 DTU's measurements predict stall already at α≈8°, while in METU's and NTNU's experiment stall kicks in a little later around α≈11°. Furthermore, somewhat higher lift values are measured in NTNU's dataset in the pre-stall region compared to the other datasets. Numerical simulations by Sagmo et al. (2016) as well as Prytz et al. (2016) point out strong 3D flow effects caused by stall cells in the pre-stall and

30   stall region. This could be a possible cause for varying experimental results in this region.

Both rotors are designed for an optimum tip speed ratio of λ_{T1}=λ_{T2}=6.0. The blades are milled from aluminium and the blade tips are cut straight. More details about the blade geometry like detailed chord and twist data is found in an invitational document by Sætran and Bartl (2015).

In this blind test experiment the model turbines are positioned at the wind tunnel center line. The upstream turbine T1's rotor plane is located at 2.00D from the test section inlet, which is verified to be far enough away to not affect the reference velocity measurement at the inlet contraction. The downstream turbine T2 is positioned 2.77D, 5.18D respectively 9.00D downstream of the upstream turbine rotor. The hub height of both turbines is adjusted to h_{hub}=0.817 m. In Fig. 3 a side cut of the wind tunnel and the wind turbine positions is shown.

2.1.3 Model turbines, rotor and airfoil characteristics

For this blind test experiment three different inflow conditions are investigated. This is supposed to shed light on the effects of various atmospheric turbulence levels as well as shear flow on wind turbine performance and its wake.

The first inflow condition investigated is a uniform inflow of very low turbulence and is from here on described as Test case A. As shown in Fig. 4 (a) there is no grid installed at the inlet of the test section resulting in a clean and uniform flow. Hot wire measurements at the upstream turbine position give a turbulence intensity level of TI=0.23% of an integral turbulent length scale of L_{uu}=0.045m. Over the rotor swept area the mean velocity in the empty tunnel is found to be uniform to within ±0.6%. The boundary layer thickness at wind tunnel walls was measured to be y_{BL}=0.200m at the upstream turbine position.

In order to investigate the effects of atmospheric turbulence on wind turbine performance and wake development, the measurements of Test case B are performed using a large scale turbulence grid at the inlet to the test section (Fig. 4. (b)). The bi-planar grid has a solidity of 35% and is built from wooden bars of 47mm · 47mm cross-section. The grid mesh size is M=0.240m, which generates a turbulence intensity of TI=10.0% at the position of the upstream turbine. The integral length scale here is assessed from an auto-correlation of a hotwire time series is calculated to be L_{uu}=0.065m at this position. The grid produces considerable spanwise variations in the flow, but as soon as the flow reaches the position of the upstream turbine T1 the mean velocity is measured to be uniform to within ±1.5% over the rotor area. Also, the turbulence intensity is assessed to be constant to within ±1.0%. In this grid generated turbulent flow the turbulent kinetic energy is decaying with increasing distance from the grid. As the flow reaches the first position of the downstream turbine T2, 2.77D downstream of T1, the turbulence intensity in the empty tunnel decays to TI=4.8% while the integral length scale is increasing to L_{uu}=0.100m.

In a third Test case C the effect of shear flow in an atmospheric boundary layer combined with atmospheric turbulence is investigated. For this purpose a large scale shear flow generating turbulence grid is installed at the inlet of the test section, as shown in Fig. 4 (c). The horizontal mesh width is constant at M_h=0.240m while the vertical mesh heights vary between $M_{v,min}$=0.016m near the floor and $M_{v,max}$=0.300m underneath the roof. The grid is bi-planar and has a solidity of 38%. As for the evenly spaced turbulence grid, it is again built from wooden bars of 47mm · 47mm cross-section. At the position of the upstream turbine T1 a turbulence intensity of 10.1% is measured at hub height. The turbulent length scale is estimated to be L_{uu}=0.097m for this case. The kinetic energy in the flow is decaying with the distance from the grid. 2.77D further

downstream the turbulence intensity has decayed to TI=5.2% while the length scale increases to L_{uu}=0.167m. At 5.18D downstream of T1 the turbulence intensity decays to TI=4.1%, while at 9.00D only TI=3.7% remain.

As wind shear and turbulence are generated only at the grid position at the tunnel inlet, their development throughout the tunnel is measured for all turbine positions. Wind shear can be described by the power law in Eq. (1), which expresses the wind speed U as a function of height z, provided that the wind speed at an arbitrary reference height z_{ref} is known:

$$\frac{U}{U_{ref}} = \left(\frac{z}{z_{ref}}\right)^{\alpha} \tag{1}$$

The power law coefficient α describes the strength of shear in the wind profile. A wind profile based on a shear coefficient of about α=0.11 is chosen for this experiment resembling the flow conditions at typical stable atmospheric conditions (Hsu et al., 1994). An exact description of the shear grid as well as the mean and turbulent flow characteristics at various positions in the wind tunnel can be found in the invitation document by Sætran and Bartl (2015).

During the present experiments the reference wind speed is kept constant at U_{ref}=11.5m/s, which is tested to give a Reynolds-number-independent turbine performance for all inflow conditions. As the downstream turbine T2 experiences significantly lower average wind speeds when operating in the turbulent wake, Reynolds number independent performance characteristics are measured down to an inflow velocity of U_{inflow}=6.0m/s at TI=5.0% background turbulence.

For Test case C, in which the velocity is increasing with height, the reference velocity of U_{ref}=11.5m/s is set at the turbine hub height h_{hub}=0.817m. This reference height is chosen for simplicity reasons; although the rotor-equivalent wind speed (Wagner et al., 2014) that represents the center of kinetic power in the shear inflow is found to be slightly below the turbine hub height (Maal, 2015).

2.2 Experimental methods

2.2.1 Power and thrust measurements

Both model turbines are equipped with a HBM torque transducer of the type T20W-N/2-Nm, which is connected to the rotor shaft through flexible couplings. In addition to that an optical photo cell is installed on the shaft giving a defined peak signal for every full rotation of the rotor. After subtracting the measured friction in the ball bearing between the rotor and torque sensor, the mechanical power on the rotor shaft can be calculated. The power on both turbines is measured and controlled simultaneously to ensure a stable operation of both turbines.

The thrust force is measured by a 6-component force balance produced by Carl Schenck AG. The drag force on the tower and nacelle structure is first measured without the rotor being present. Thus, it is possible assessing the rotor thrust by subtracting the tower-nacelle drag from the total drag.

2.2.2 Wake flow measurements

The mean and turbulent velocities in the wake behind the upstream turbine T1 are measured by a single hot-wire anemometer (HWA) in constant temperature mode (CTA). Each measurement point is sampled for 45s at 20kHz resulting in a total of $9.0 \cdot 10^5$ samples. The signals are amplified and filtered appropriately to avoid the distortion by noise etc. All the wake measurements are repeated using a two-component Laser Doppler Anemometry (LDA) system by Dantec Dynamics for verification. A time series of $5.0 \cdot 10^4$ samples is sampled for a varying period of about 30 seconds. The reference velocity U_{ref} used for normalization of the mean and turbulent wake velocity as well as the non-dimensional power and thrust coefficients is measured at the inlet contraction of the wind tunnel. The pressure difference around the circumferences of two defined cross sections is logged simultaneously for every measuring point. The air density ρ in the experiment is calculated from the measured air temperature and atmospheric pressure in the test section for every measurement point.

2.2.3 Measurement uncertainties

The statistical uncertainty of every sample of the power, thrust and mean velocity measurements is calculated following the procedure proposed by Wheeler and Ganji. (2004). Random errors are computed from the standard deviations of the various measured signals on a 95% confidence interval. Taking also systematic errors from the calibration procedures into account by following the procedure of Eriksen (2016), a total error is calculated. Herein, the systematic error of about ±1.0% from the velocity calibration is seen to be the major contributor to the total uncertainty. The uncertainty in the turbulent quantities in the wake flow is calculated according to the approach by Benedict and Gould (1996).

The uncertainty in the upstream turbine power coefficient at design conditions is calculated to be within ±3.0%, while it is lower than ±2.0% for the thrust coefficient. It is observed that the uncertainty of the mean velocity is somewhat larger in the freestream outside the wake. At higher velocities the sensitivity of the hot-wire probe is smaller which is giving higher uncertainties. The measured values of the turbulent kinetic energy are observed to feature the highest uncertainty in the shear layer between wake and freestream flow.

2.3 Computational contributions

2.3.1 Uppsala University and DTU (UU-DTU)

S. Sarmast, *R. Mikkelsen* and *S. Ivanell* from Uppsala University, Campus Gotland, Sweden and DTU, Campus Lyngby, Denmark contributed with a dataset simulated by Large Eddy Simulations (LES) combined with an Actuator Line (ACL) approach. The DTU-in-house code EllipSys3D, which is based on a multiblock finite volume approach, was used to solve the Navier-Stokes computations. The convective terms are herein discretized by a combination of a third order and a fourth order scheme. The time domain is discretised that the tip movement of a rotor blade is less than a half cell size per time-step.

The flow field around the wind turbine rotor was simulated using the actuator line technique developed by Sørensen and Shen (2002). Herein, the Navier-Stokes equations are solved with body forces distributed along rotating lines representing the blades of the wind turbine. The lift and drag coefficients are taken from the previously mentioned self-generated dataset for the NREL S826 airfoil by Sarmast and Mikkelsen (2013). For each of the 43 blade points the forces are interpolated for

5 the local Reynolds numbers in a range of 40000 to 120000. Additionally, a force line is introduced account for the drag force generated by the tower. The wake flow field is calculated by solving the Navier-Stokes equations using LES with an integrated sub-grid scale (SGS) viscosity model.

A regular Cartesian grid which is divided into 875 blocks makes out the computational domain. With 32 points in each block and 43 points representing each blade a total of 28.6 million mesh points is used to simulate the various test cases. This

10 resolution was tested to give a grid-independent simulation result.

The inlet turbulence is modelled by implanting synthetically resolved turbulent fluctuations 1.5D upstream of the position of the upstream rotor T1. These fluctuations from a pre-generated turbulence field are superimposed to the mean velocities through momentum sources yielding isotropic homogenous turbulence. The mean and turbulent profiles of the different test cases are tested to give a good match with the corresponding wind tunnel values. In addition, the effect of shear flow in an

15 atmospheric boundary layer combined with atmospheric turbulence is investigated. The shear profile is implemented to match the profile given in the invitational document by Sætran and Bartl (2015). A more detailed description of the method can be found in Sarmast et al. (2014).

2.3.2 Vrije University Brussels (Vrije)

20 *N. Stergiannis* from Vrije University and Von Karman Institute (VKI) in Brussels, Belgium, performed Reynolds Averaged Navier Stokes (RANS) simulations using the open source software package OpenFoam in combination with a Multiple Rotating Frame (MRF) approach. Therein, the full rotor geometry is resolved in its own frame of reference and the flow calculated around the "frozen rotor". The subdomain is connected to the stationary frame of reference by an Arbitrary Mesh Interface (AMI). A grid independency test was executed investigating different cell sizes, giving an independent result with a

25 total number of $3.5 \cdot 10^7$ cells. Slip conditions are used at the wind tunnel walls, which was deemed to save computational effort and still takes into account the blockage effect generated by the walls. The rotor and the nacelle are completely resolved, but the turbine towers are not simulated in the final computations. The boundary layers on the blades and nacelle are resolved down to a $y^+ \approx 30$. The standard k-ω turbulence model as implemented in OpenFOAM v.2.4 is applied for the presented simulations. The mean and turbulent inlet velocities were matched with the experimental values provided in the

30 invitational document. As the blade forces could not be directly extracted from the fully resolved rotor simulations, a Blade Element Momentum (BEM) code based on the method by Ning (2014) is used to calculate the power and thrust characteristics of the model wind turbines. The lift and drag coefficients are computed with the open source software XFoil (Drela, 2013) for the NREL S826 airfoil at all prevailing Reynolds numbers. The reference velocity for the downstream

turbine is calculated as the average velocity over a line of one radius 1D upstream of the downstream rotor. Only test cases A and B are modelled.

2.3.3 Łódź University of Technology (LUT)

5   *M. Lipian*, *M. Karczewski* and *P. Wiklak* from the Institute of Turbomachinery at Łódź University of Technology, Poland, contributed with two data sets computed by the commercial CFD software Ansys CFX. All simulations were performed to find a steady state solution of the RANS equations using the k-ω SST model for turbulence closure.

For the test cases A, B and C they fully resolved the rotor geometry. Thus, the solver resolves the actual flow around the rotor and no additional assumptions needed to be made. These simulations will be denoted as Fully Resolved Rotor Model

10   **LUT (FRR)** from now on. Two rotating sub-domains are established around the rotors while the main wind tunnel domain is stationary. A structural mesh is created with the software ICEM CFD to discretise the domains. The wind tunnel is discretised by a total number of $3.0 \cdot 10^4$ plus two refined subdomains around the rotors of $6.0 \cdot 10^3$ nodes each. A grid independence test was executed for the rotor sub domain to prove grid-independent convergence.

For the test cases B_1, B_2 and B_3 a different approach was chosen. The rotors are represented by a custom-made Actuator Line

15   model which will be denoted as **LUT (ACL)**. Herein, the blades are modelled as parallel-epipedons, representing a sub-domain in which the RANS equations are modified. The flow is modified by an addition of force components, which are calculated from tabulated lift and drag data dependent on the local chord and angle of attack. The lift and drag data is taken from the invitational document and was originally created with XFoil. The ACL model furthermore includes a Prandtl tip loss correction. For these test cases an unstructured mesh is used in the wind tunnel main domain and parallel-epipedon,

20   discretized by a total number of $1.7 \cdot 10^6$ nodes in the main domain plus two times $1.0 \cdot 10^6$ nodes in the sub-domains around the rotors.

As the test cases B and B_2 are identical, a direct comparison between the performance and wake results of the FRR and ACL simulations is possible.

2.3.4 CD-adapco (CD-adapco)

25

S. Evans and *J. Ryan* from CD-adapco, London, United Kingdom, contributed with a full data set of predictions simulated by Improved Delayed Detached Eddy Simulations (IDDES). The IDDES Spalart Almaras turbulence model is used for turbulence closure in the boundary layers. Both the meshing and the actual simulation is carried out with their commercial software package STAR-CCM+, which is a finite-volume solver using cells of arbitrary shape.

30   Besides the turbine rotors, the exact geometry of the turbine nacelles, towers and wind tunnel walls is modelled. The computational domain is divided into 3 sub-domains. In the main wind tunnel domain a hexahedral dominant grid is applied, which is further refined around the turbines and in the wake region. In the disc shaped regions around the rotors an isotropic

polyhedral mesh of even finer resolution is utilised. The boundary layers around the blade surfaces are resolved down to a $y^+<2$. The rotating disk domains around the turbine rotors are connected to the main domain via an arbitrary sliding interface. For the entire computational domain around $2.5 \cdot 10^7$ grid cells are applied.

5   The inlet conditions are modelled with the Synthetic Eddy Method, generating an inflow field of defined turbulence intensity and length scales that are corresponding to the values given in the invitational document. For test case C, an atmospheric boundary layer is defined by a power law at the wind tunnel inlet. Explicit transient modelling is used to simulate the wind turbine interactions while the turbines' rotations are modelled as a rigid body motion. A transient 2nd order model with a time step of $dt=1.0 \cdot 10^{-4}$s is used. Advanced limiter options for minimum limiting and higher order spatial schemes are used in a segregated solver. The transient calculation is run for 1s in test cases A, B_1, B_2 and C respectively 2.5s in test case B_3 due to

10   the higher separation distance. The required values are thereafter averaged for a time period of 0.5s.

More information about the use of Star-CMM+ in rotating flows can e.g. be found in Mendonça et al. (2012).

2.3.5 CMR Instrumentation (CMR)

A. Hallanger and *I.Ø. Sand* from CMR Instrumentation in Bergen, Norway, provided a data set based on RANS simulations

15   combined with a BEM approach. For the calculation of the mean and turbulent flow quantities their in-house CFD code called Music was used. The RANS equations are solved with a standard k-ε model with Launder-Spalding coefficients. Furthermore, a sub-grid turbulence model is applied to represent the rotor generated turbulence. Therein, it is assumed that the production rate of turbulent kinetic energy and its rate of dissipation are integrated over the wake of the wind turbine and distributed over the near field. Convective and diffusive fluxes are approximated with the second order Van Leer (1974) and

20   central difference schemes. The turbulent intensity and length scales at the inlet are specified according to the experimental values given in the invitational document for the three different test cases. For test case C, a power law profile is used.

The rotors are included as sub-models in the CFD code. They are represented by their reaction forces on the flow field. The blade forces are simulated by a BEM code including wake rotation. The blades are divided into 30 blade elements in radial direction. The BEM code includes the Prandtl tip-loss correction as well as Glauert's empirical model for highly loaded

25   rotors. The lift and drag coefficients were calculated from the software XFoil (Drela, 2013) in dependence of angle of attack, Reynolds number and relative turbulence intensity. Therein, the transition amplification numbers (N_{crit}) are representing the turbulence intensity levels present at the different positions in the wind tunnel. 3D corrections for 2D force coefficients according to the BEM method by Ning (2014) were applied. These forces were used as source terms in for axial and rotational momentum conservation. The turbine hubs and towers were modelled as flow resistances in the same control

30   volume as the rotors. Turbine hubs were represented by a drag coefficient of $C_{D,hub}=0.6$, while the tower drag is approximated by $C_{D,tower}=1.2$.

Wind tunnel walls were modelled by wall functions. The entire wind tunnel environment including the two rotors was resolved in a total of $5 \cdot 10^5$ structured grid nodes. Steady state simulations of the blade forces were performed with an angular

increment of 15° resulting in a total of 24 azimuthal positions of the turbine rotors. This was deemed to be sufficient to include the effects of shear flow on the first turbine. A detailed description of the computational methods applied is given in Hallanger and Sand (2013).

5   **2.4 Required output**

In total five different test cases are provided for simulation in this blind test experiment. An overview of the turbines' operating conditions, positioning as well as measurement station of the wake measurements is shown in Table 1.

2.4.1 Wind turbine performance

10   For all five test cases the power coefficients $C_{P,T1}$ and $C_{P,T2}$ (Eq. 2) as well as the thrust coefficients $C_{T,T1}$ and $C_{T,T2}$ (Eq. 3) of both turbines are compared:

$$C_{P,T1/T2} = \frac{8\,P_{T1/T2}}{\rho\,\pi\,D_{T1/T2}^2\,U_{ref}^3} \tag{2}$$

$$C_{T,T1/T2} = \frac{8\,F_{T1/T2}}{\rho\,\pi\,D_{T1/T2}^2\,U_{ref}^2} \tag{3}$$

Herein, $P_{T1/T2}$ denotes the mechanical power on the turbine shaft, $F_{T1/T2}$ the thrust force in streamwise direction on
15   the rotor and ρ the air density. The upstream turbine T1 is operated at a tip speed ratio of $\lambda_{T1}=\omega\cdot D_{T1}/2\cdot U_{ref}=6.0$, whereas the downstream turbine T2 is run at $\lambda_{T2}=\omega\cdot D_{T2}/2\cdot U_{ref}=4.5$. Note, that the same reference velocity U_{ref} defined at the test section inlet is used for both turbines. The optimal tip speed ratio for the downstream turbine T2 is also $\lambda_{T2}=\lambda_{T1}=6.0$ when the turbine is unobstructed. As T2 operates in the wake the actually experienced velocity is considerable lower reducing also the optimal rotational speed and thus the tip speed ratio λ_{T2}. The optimal tip speed ratio at which
20   the maximum power P_{T2} is achieved, in fact varies between $\lambda_{T2}=4.0$-5.0 depending on the turbine separation distance x/D and inlet turbulence level TI_{Inlet}. For better comparability a fixed tip speed ratio of $\lambda_{T2}=4.5$ was chosen.

2.4.2 Mean and turbulent wake flow

Furthermore, the horizontal profile of the mean and turbulent flow is compared at the pre-defined wake measurement
25   positions (Table 1). The upstream turbine is still operated at $\lambda_{T1}=6.0$ for all five test cases. The profiles of the normalized mean velocity U* (Eq. 4) and the normalized turbulent kinetic energy k* (Eq. 5) are to be calculated at the turbine hub height $h_{hub}=0.817$m:

$$U^* = U/U_{ref} \tag{4}$$

$$k^* = k/U_{ref}^2 \tag{5}$$

In a cylindrical coordinate system the turbulent kinetic energy k is defined as (Eq. 6):

$$k = \tfrac{1}{2}(u_x'^2 + u_r'^2 + u_\theta'^2) \tag{6}$$

5   Since only two of the normal stresses are actually measured the isotropic normal stress approximation (Eq. 7) is used to determine the turbulent kinetic energy in each measurement point:

$$k = \tfrac{3}{2}u_x'^2 \tag{7}$$

Krogstad et al. (2014) showed that the turbulence in the wake of the model turbine is very isotropic. They measured all three components of the stress tensor for one wake profile at x/D=1 and demonstrated a very good agreement of k calculated from
10   all three normal stresses with the estimated k calculated with only u_x' and the isotropic turbulence relation.

3 Results

The comparisons of the predictions and experimental results are analysed for the different inflow conditions. In chapter 3.1 power, thrust and wake predictions for test case A (low turbulence inflow) are presented. Thereafter, all the test cases for
15   high turbulence inflow conditions for all three separation distances (test cases B_1, B_2. B_3) are analysed in chapter 3.2. Finally, the results of test case C, featuring a highly turbulent shear flow, are compared in chapter 3.3.

Experimental results for power and thrust are indicated by filled black circles for the upstream turbine and empty circles for the downstream turbine. The measurements of the wake profiles with Hot-wire anemometry (HWA) are marked with filled black circles, while flow measurements with Laser-Doppler Anemometry (LDA) are indicated by grey filled circles. The
20   different contributions of numerical simulations are assigned one consistent symbol and colour for power, thrust and wake flow predictions.

3.1 Test case A: low turbulence uniform inflow

3.1.1 Power and thrust predictions

25   The power and thrust predictions for test case A (low turbulence inflow, TI=0.23%) from the five contributions are compared to the experimental results in Fig. 5. The respective numerical values are listed in Table 2.

The experimentally measured power coefficient of the upstream turbine has its maximum $C_{P,max}=0.462$ at $\lambda=6.0$ and its runaway tip speed ratio at $\lambda=11.1$. At a turbine tip speed ratio of about $\lambda=3.5$ a rapid transition of $C_{P,T1}$ into stall is observed. The predictions of the power coefficient of the upstream turbine T1 at its design operating point $\lambda_{T1}=6.0$ show a scatter of about $\pm7\%$ compared to the measured $C_{P,T1}$. This points out significant differences in the modelling methods. While CMR
5   generated a Reynolds-dependent dataset for lift- and drag coefficients using the airfoil design and analysis code XFoil (Drela, 2013) as an input for their BEM model, UU-DTU used an experimentally generated lift and drag dataset produced by Sarmast and Mikkelsen (2013) as an input for their ACL model. Another aspect is how the predictions modelled the influence of solid wall blockage on the C_P values. As the flow cannot expand freely around the turbine, the induction is reduced, resulting in higher power production of the turbine than that in an unblocked flow. All five contributions took the
10   wind tunnel boundaries into account resulting in fairly well approximations of the upstream turbine's C_P at design conditions.

The scatter in C_P for the downstream turbine T2 is considerably larger than for T1. T2 is operated around its design point at $\lambda_{T2}=4.5$ (referred to U_{ref} measured upstream of T1) in the wake at a separation distance of $x/D_{T2}=5.18$ from the upstream turbine T1. The power is underestimated by up to 25% and overpredicted more than 30% at the most. Some predictions,
15   however, such as CMR, LUT and CD-adapco manage to match the experimental result reasonably well, overestimating the downstream turbine power by only 9-17%, which is a rather small deviation given the large scatter of more than 100% as observed in previous blind test experiments (Pierella et al., 2013), (Krogstad et al., 2014).

The predictions of the thrust coefficient for turbines T1 and T2 give a similar picture, as shown in Fig. 5 (b). Even though the upstream turbine thrust is slightly underpredicted by most simulations, the scatter is significantly smaller than in earlier
20   Blind tests. The C_T predictions for the downstream turbine show approximately the same scatter as the upstream turbine. The BEM predictions by CMR matched the experimental results very closely for both turbines.

3.1.2 Wake predictions

For the low inlet turbulence test case A, predictions of the wake flow at $x/D_{T2}=2.77$ behind the upstream turbine are
25   compared. Horizontal profiles of the normalized mean velocity U^* and the normalized turbulent kinetic energy k^* are compared at hub height.

As already observed in a very similar test case in Blind test 1 (Krogstad and Eriksen, 2013) the mean velocity profile at $x/D=2.77$ features two distinct minima located behind the blade tips of the rotor. The evident asymmetry in the wake center is caused by the advection of the tower wake into the swirling rotor wake as shown in rotor wake experiments by Schümann
30   et al. (2013). As presented in Fig. 6 (a) the general wake shape and level of velocity deficit are well predicted by UU-DTU, CD-adapco and the fully resolved rotor simulations by LUT. However, the vertical wake extension as modelled by LUT is too small for this low turbulence inflow test case. CD-adapco's IDDES simulations manage to capture the shape of the wake profile very well, including the asymmetries caused by the tower wake in the center of the profile. CMR's RANS

simulations based on a k-ε turbulence model predict a Gaussian wake shape with only one minimum already at x/D=2.77 downstream of the rotor, suggesting a more homogenous flow as measured in the experiments. Integrating over CMR's wake profile, however, gives a fair estimate of the kinetic energy contained in the wake flow. Vrije's MRF method does not resolve the details in the mean velocity profile as the turbine tower was not included in the simulation. The velocity deficit in

5   the wake is significantly underestimated; in average it amounts only about 50% of the experimentally measured values.

The normalized turbulent kinetic energy profiles are compared in Fig. 6 (b). The experimental profile shows two distinct peaks in the shear layer generated by the tip vortices around z/R=±1. A third, but substantially smaller peak slightly left to the wake center is ascribed to the turbulence generated by the tower and nacelle structures. It can be observed that the turbulent kinetic energy in the shear layer is significantly underpredicted by all models. This has previously been observed in

10   Blind test 1 (Krogstad and Eriksen, 2013) where the turbulent kinetic energy predictions were one or more magnitudes too low for a low background turbulence. In the present test case, however, three of the five models give results of the correct magnitude. Both, UU-DTU's LES model and CD-adapco's IDDES simulation show a good agreement in the profile shape, only underpredicting the peaks in the shear layer by about 30%. CMR's simulation shows two peaks of about the same magnitude as the aforementioned models. However, the local turbulence peaks seems to be smeared out into the center of the

15   wake as well as the freestream flow (z/R=1.5-2.0). LUT's RANS simulation based on the k-ω SST turbulence model shows three distinct peaks, but underpredicts the turbulence levels by almost one magnitude. Vrije's MRF simulations based on a k-ω turbulence model reproduce the peaks in the shear layer; the predictions are however about one third of the experimental values in the shear layer. In the unaffected freestream flow, however, the turbulence values are predicted more than one magnitude too high by Vrije's model.

20

3.2 Test case B: high turbulence uniform inflow

3.2.1 Power and thrust predictions

A second set of power and thrust predictions is compared for inflow conditions of higher turbulence. A turbulence grid installed at the wind tunnel inlet is generating a uniform wind field with a turbulence intensity of TI=10.0% at the location of

25   the first turbine rotor. For this high background turbulence level the turbine power and thrust are compared for three turbine separation distances x/D= 2.77, 5.18 and 9.00 (test cases B_1, B_2 and B_3). The power and thrust predictions for test case B are compared in Fig. 7 (a)-(f). A comparison of the respective numerical values is presented in Table 3.

Comparing the upstream turbine power curve for high background turbulence (test cases B_2, Fig. 7 (c)) to the upstream turbine power curve of low background turbulence (test case A, Fig. 5 (a)) a very similar curve shape is observed. At

30   increased background turbulence the maximum power coefficient is measured at the same level as for low background turbulence. Also, the runaway tip speed ratio at λ=11.4, at which the rotor does no longer produce energy, is very similar for

both inlet turbulence levels. The most noticeable difference is the transition to stall at a tip speed ratio of about λ=3.5 and lower. For higher background turbulence the transition into stall is much smoother compared to low inlet turbulence.

The predictions of $C_{P,T1}$ at its design operating point $λ_{T1}$=6.0 are again very accurate, scattering only about ±7% around the experimental value. Also, the predictions of the thrust coefficient $C_{T,T1}$ are matching very well. As previously observed in

5   test case A, the $C_{T,T1}$ is slightly under predicted, in this case up to -9% at its most. Comparing the performance results of the downstream turbine, the best predictions are made for the lowest turbine separation distance x/D=2.77 (test case B_1, Fig. 7 (a)). The experimentally measured power coefficient $C_{P,T2}$ is well matched, with a total deviation of about ±15%. The downstream turbine thrust coefficient $C_{T,T2}$ is predicted within ±10% by all the modellers in test case B_1. The predictions by CMR and CD-adapco match the experimental results closest.

10 Increasing the turbine separation distance to x/D=5.18 in test case B_2 the scatter in the results becomes significantly larger (Fig. 7 (c)). The scatter in the downstream turbine power coefficient $C_{P,T2}$ increases to about ±20% in both directions. The fully resolved rotor model (FRR) by LUT results in a very good prediction of the downstream turbine power coefficient, while their actuator line model (ACL) overpredicts the power significantly. This can be directly related to different wake flow predicted by the two models. The wake flow acts as inflow for the downstream turbine (compare Fig. 8 (a) further

15 down). In contrary, UU-DTU's Ellipsys3D calculation underpredicts the downstream turbine performance significantly, even though the wake characteristics are predicted very accurately. Also Vrije underpredicts the downstream turbine power significantly. This is rather surprising as the wake deficit at x/D=5.18 is slightly underpredicted as well and more power should be left in the flow for the downstream turbine. The scatter in the thrust calculations is in general smaller than for the power predictions for all models, with most simulations underpredicting the experimental value. The thrust coefficient is less

20 sensitive to a correct prediction of the incoming velocity field than the power coefficient. The thrust coefficient is indirectly proportional to the incoming velocity squared ($\sim U_{ref}^2$), while the power coefficient is even more sensible to an incorrect prediction of the incoming velocity field ($\sim U_{ref}^3$). Surprisingly, LUT's FRR model gives the smallest value for the downstream turbine thrust coefficient, although the power and wake predictions for this downstream distance are matching the experimental results very well.

25 With a further increase in turbine separation distance to x/D=9.00 (test case B_3) the experimentally measured downstream turbine power coefficient recovers to $C_{P,T2}$=0.270. The variation in the simulations is seen to be even bigger for this downstream distance reaching a scatter of more than 30%. The same trend as already seen for smaller separation distances is observed: UU-DTU's and Vrije's simulations are clearly underpredicting the power coefficient, while LUT's ACL model is overestimating the downstream turbine power considerably. The thrust predictions show similar tendencies as the power

30 predictions but are seen to match the experimentally measured value better.

3.2.2 Wake predictions

For the high background turbulence test case B, the participants were asked to predict the mean and turbulent wake characteristics at three downstream distances x/D_{T2}=2.77, 5.18 and 8.50. Note that the horizontal wake profiles were extracted from test case B_3 where the downstream turbine T2 was installed at x/D_{T2}=9.00 and operating at λ_{T2}=4.5. The wake

5   flow as measured at x/D_{T2}=8.50 is therefore experiencing the induction of the downstream turbine which is located only x/D_{T2}=0.50 further downstream. The horizontal wake profiles of the normalized mean velocity U/U_{ref} and normalized turbulent kinetic energy $k^*=k/U^2_{ref}$ are compared in Fig. 8 (a)-(f).

The wake characteristics of the flow x/D_{T2}=2.77 downstream of T1 are presented in Fig. 8 (a) and (b). For this case, LUT simulated the wake flow with two different models, the simpler actuator line model (ACL) and the computationally more

10   expensive fully resolved rotor (FRR) model. At this downstream distance the mean wake profiles are characterized by two distinct minima. The experimental results clearly show that a Gaussian wake shape has not yet developed. A very accurate prediction of the mean wake shape is given by UU-DTU's simulation, but also CD-adapco and the FRR model by LTU capture the shape very well. LTU's ACL model, however, only predicts one distinct minimum in the mean wake profile. Only one minimum is also predicted by CMR while the mean velocity profile is rather skewed. Vrije's simulations match the

15   experimental measurements significantly better for a higher background turbulence level than for the lower turbulence level of Test case A, predicting both the level and wake shape fairly well.

Very good predictions of the distribution of the turbulent kinetic energy are presented by UU-DTU as well as CD-adapco. Both simulations predict the magnitude and location of the two peaks around $z/R=\pm1$ as well as the region of lower turbulence into the center of the wake very accurately. LUT's FRR simulation manages to reproduce the general shape of the

20   turbulence profile, but the levels are about 50% below the measured turbulence values. Similar levels are observed for LUT's ACL simulation, which is additionally smearing out the turbulence to the center of the wake. It has been discussed that the tip loss correction model included in the ACL model could have contributed to kill the turbulent peaks. Vrije's model based on a standard k-ω turbulence model underpredicts the peaks in the shear layer significantly; they are observed to be lower than the turbulence levels in the freestream flow, which are overpredicted by more than one magnitude. CMR's

25   simulations predict too high turbulence levels both at the peaks, in the center and at the wake boundaries. CMR's simulations are based on the k-ε turbulence model, which is predicting a far too blurry turbulence distribution for this case.

Moving downstream to x/D_{T2}=5.18 a more Gaussian mean velocity profile with only one distinct minimum develops as shown in Fig. 8 (c). The general shape of the mean velocity profile is in this case well predicted by almost all the simulations; only Vrije's simulation indicates a near-wake shape with two minima. Again, UU-DTU's model is giving the

30   best match with the experimentally measured profiles. CMR's model computes a slightly asymmetric mean wake profile underpredicting the velocity deficit somewhat. LUT modelled the 5.18D wake using their simpler ACL model, which is underpredicting the mean velocity deficit considerably. CD-adapco's IDDES simulation overpredicts the mean wake velocity deficit to some extent, which was previously indicated in the 2.77D wake profile. The turbulence profiles for

x/D_{T2}=5.18 as presented in Fig. 8 (d) show a similar picture as seen for x/D_{T2}=2.77. The best predictions are made UU-DTU's LES simulation. CD-adapco's IDDES computation is also predicting the overall shape fairly well, but the turbulence peaks in the tip vortex region at z/R=±1.0 are clearly overpredicted. Compared to the profiles at 2.77D the peaks do not really decrease, meaning that there is almost no turbulence decay from 2.77D to 5.18D predicted. Too smooth turbulence profiles are predicted by CMR as well as LUT's ACL model, clearly overpredicting respectively underpredicting the mean turbulence levels.

A challenging test case is shown for the wake measured at downstream position x/D_{T2}=8.50, only half a rotor diameter upstream of the rotor of T2 (Fig. 8 (e) and (f)). A smooth Gaussian mean velocity profile has developed while velocity deficit is further decreasing. One might assume that the induction of the downstream turbine T2 is further reducing the mean velocity field. Measurements with and without the downstream turbine installed confirmed a further reduction in mean velocity. However, the presence of the downstream turbine reduces the mean velocity by only about 5% (not shown in graph). Again, UU-DTU is predicting the mean wake well. Although, the mean profile predicted from LUT's ACL model is matching the experimental values very well for this case it is very similar to the profile predicted already for 5.18D, where it was clearly underpredicting the velocity deficit. CD-adapco's simulation is strongly overpredicting the mean velocity deficit in the wake at this downstream distance. Surprisingly, the mean velocity deficit even grows noticeably in comparison to the mean wake profile predicted at 5.18D. Also Vrije's MRF simulation overpredicts the mean velocity deficit for this case. Surprisingly, the mean wake profile at 8.50D is very similar to the one predicted at 5.18D also in Vrije's predictions. As observed for smaller downstream distances already, CMR predicts a too low velocity deficit also for 8.50D. Analysing the turbulence profile as shown in Fig. 8 (f) the tip vortex peaks have decayed to about 50% of the level measured at 5.18D. Both CD-adapco's IDDES as well as UU-DTU's LES simulation give a fairly well approximation of the turbulence profile. CMR is overpredicting the turbulence levels at 8.50D, while LUT's ACL model is underpredicting the turbulence considerably. The turbulence levels predicted by Vrije's k-ω model at 8.50D are observed to be very similar to those already predicted at lower separation distances. This indicates that the turbulent decay rate is not well captured for this case.

3.3 Test case C: high turbulence non-uniform shear flow

3.3.1 Power and thrust predictions

For the last test case the complexity of the inflow conditions is increased. The inflow to the test section is no longer spatially uniform. Another custom-made grid with vertically increasing distance between the horizontal bars is placed at the test section inlet generating a shear flow that can be approximated by the power law exponent α=0.11. The background turbulence of this grid is measured to be TI=10.1% over the rotor area at the location of the first turbine rotor. This makes the effects of shear flow well comparable to test case B as basically the same background turbulence level is predominating. For test case C the turbine power and thrust are compared only for one turbine separation distance x/D_{T2}=5.18. The power

and thrust predictions for the shear flow test case are presented in Fig. 9 while the exact numerical values are shown in Table 4.

Comparing the upstream turbine power curve of test case C (Fig. 9 (a)) to the upstream turbine power curve of uniform inflow test case B (Fig. 7 (c)) a very similar curve shape is observed. Taking a closer look, however, a slightly lower maximum power coefficient is measured in case C and a marginally earlier run-away point is found at λ=11.2. This is assumed to stem from the fact that the reference velocity U_{ref} for this test case is defined at the center of the rotor at hub height. Due to the vertically non-linearly increasing velocity distribution, the rotor equivalent wind speed (Wagner et al., 2014) is found to be different from U_{ref} measured at hub height. As the gradient in the shear flow is higher for the lower half of the rotor are than for the upper half, the rotor equivalent wind speed is found marginally lower than at hub height. A re-calculation of the C_P curve measured in shear flow with the slightly lower rotor equivalent wind speed (not shown in this report) is giving an almost exact match with the C_P curve for uniform inflow as presented in test case B.

The predictions of $C_{P,T1}$ at the turbines design operating point λ_{T1}=6.0 are again very precise, showing a scatter of less than ±5% from the measured value. All the contributions predict a little lower $C_{P,T1}$ value as in test case B confirming the tendency measured in the experiment. Also, all the predictions of the thrust coefficient $C_{T,T1}$ give a very good match with the experiment. In this case the spread is about ±5% which is just slightly outside the measurement uncertainty.

Analysing the performance results of the downstream turbine at x/D_{T2}=5.18 yet the predictions are very good. The scatter in $C_{P,T2}$ is within ±7%, except from UU-DTU's prediction that is about 24% lower than the experimental value. This seems to be a systematic deviation as significantly low values have been observed in test cases B already. The predictions of the thrust coefficient are very close to each other, however up to 16% lower than the measured value at λ_{T2}=4.5. A general tendency in underpredicting the thrust is again seen for all test cases (A, B, C), but the predictions are significantly closer compared to previous blind test comparisons.

3.3.2 Wake predictions

One single wake profile behind the upstream turbine is compared for test case C in which the turbine is exposed to highly turbulent shear flow at the test section inlet. The mean and turbulent wake characteristics at x/D_{T2}=2.77 behind the upstream turbine are compared in Fig. 10.

The mean velocity profile (Fig. 10 (a)) has a very similar shape as the wake behind the same turbine exposed to uniform inflow of the same turbulence intensity (Fig. 8 (a)). Also the mean velocity profile for shear inflow is characterized by two distinct minima and a smooth transition from the wake to the freestream. Taking a closer look the wake in case C is slightly skewed compared to the one measured in test case B. Especially the minimum velocity peak at z/R≈-0.7 is somewhat lower as in test case B. It is assumed that low kinetic energy fluid that encounters the lower half of the rotor is transported into the measurement plane by the rotation in the wake. Turbulent mixing processes have most likely evened out this effect already at x/D=2.77, yet a small difference is detectable.

Four different predictions are compared as Vrije did not simulate test case C. As observed for the earlier test cases, UU-DTU's LES simulation predicts the mean wake shape very accurately. The levels of the two minima are matched very closely. LUT's fully resolved rotor simulation gives a good agreement as well; the skew in the wake is however not as distinct as in the measured profile. CD-adapco predicts the skewed shape of the wake very well; the kinetic energy deficit

5   however is again slightly too high in the blade tip regions. As previously observed for test case B the two mean velocity minima are melted into only one in CMR's simulations. The skew in the mean wake profile is also observed for this simulation when comparing to CMR's mean wake prediction for test case B.

Analyzing the turbulent kinetic energy profiles for test case C (Fig. 10 (b)) obvious similarities to the ones of test case B (Fig. 8 (b)) are observed. UU-DTU's simulations match the experimental results very accurately in the center and the tip

10   region, whereas the turbulence level in the freestream is slightly too high. LUT's FRR simulations underpredict one peak significantly while the turbulence level in the freestream is significantly higher than in the measurements. The TKE predictions by CD-adapco give an almost perfect fit with the experiments in this case. The center region, turbulence peaks in the shear layer as well as the freestream level match the measured profiles very well. Similar observations as in test case B are made for the turbulence predictions of CMR. Although the shear layer peaks are on the same level as the experimental

15   values are the levels of turbulence in the center of the wake as well as in the freestream clearly too high.

4 Conclusions

Five different research groups predicted the performance and wake flow between two in-line model wind turbines with a number of different simulation methods. The methods cover different approaches, ranging from commercial software to in-

20   house developed codes. The effect of three different inflow conditions, low turbulence uniform inflow (A), high turbulence uniform inflow (B) and high turbulence non-uniform shear inflow (C) are investigated.

The performance of the upstream turbine ($C_{P,T1}$, $C_{T,T1}$) was commonly predicted rather well by all predictions for all three inlet conditions, with an acceptable scatter of ±5% to ±7% depending on the test case. The upstream turbine's performance was however well-known from earlier Blind tests. The scatter in the performance data of the downstream turbine at design

25   conditions is generally observed to be larger. For 5.18 rotor diameters separation distance the $C_{P,T2}$ predictions varied within ±20%. By decreasing the separation distance to 2.77D the deviations from the measured results reduced to ±15%, while an increase in separation distance to 9.00D resulted in an even bigger scatter of ±30%. The scatter in the predictions of the downstream turbine thrust coefficient are generally seen to be smaller than in the power coefficient and a tendency of underpredicting the measured value is observed. Nevertheless, a significant improvement in the predictions of downstream

30   the turbine's performance is observed compared to earlier Blind test experiments where the scatter was more than ±100% (Pierella et al., 2013) respectively ±50% (Krogstad et al., 2014).

Comparing wake profiles behind the upstream turbine it can be concluded that UU-DTU's LES simulation delivers very accurate predictions of the experimentally measured mean and turbulent characteristics for all freestream conditions and separation distances. Also the predictions based on the IDDES model by CD-adapco resolve the mean and turbulent structures in the wake very well with a tendency to predict a marginally too high wake velocity deficit. The mean wake profiles are well predicted by the fully resolved k-ω SST simulations by LUT, whereas the turbulence is seen to be underpredicted. Simulations by the same group based on an actuator line approach are observed not to resolve the flow structures in sufficient detail. Similar conclusions can be drawn to CMR's wake predictions based on the k-ε turbulence model. The levels of mean velocity deficit are mostly approximated reasonably well; the details are however often lost due to an overprediction of turbulent diffusion. This might be also the case for the k-ω simulations by Vrije in which acceptable approximations of the mean velocity deficit for high background turbulence are predicted, while the predicted turbulence distributions are observed to be too smooth.

In general, it can be concluded that both performance and wake were predicted better for a higher background turbulence level than for the low turbulence laboratory conditions. The challenges of the more complex non-uniform shear flow were solved fairly well by most of the simulations, as most of them were able to predict a slightly skewed wake.

The discussion in the workshop disclosed that the quality of the wake predictions is dependent not only on the turbulence model, but rather a complex combination of user-dependent factors. This could be e.g. different methods of meshing, choice of turbulence parameters or force coefficients for rotor modelling. Nevertheless, this blind test also confirms that it is possible to make very accurate performance and wake flow predictions given the model and input parameters are chosen correctly.

Acknowledgements

References

Adaramola, M.S., and Krogstad, P.Å.: Experimental investigation of wake effects on wind turbine performance, Renewable Energy, 36 (8), 2078–2086, doi:10.1016/j.renene.2011.01.024, 2011.

Ainslie, J.F.: Calculating the flowfield in the wake of wind turbines, Journal of Wind Engineering and Industrial Aerodynamics, 27 (1–3), 213-224, doi:10.1016/0167-6105(88)90037-2, 1988.

Aksnes, N.Y.: Performance Characteristics of the NREL S826 Airfoil - An assessment of Re-independency and effect of inflow turbulence, Master's thesis NTNU, 2015.

Barthelmie, R.J., Hansen, K., Frandsen, S.T., Rathmann, O., Schepers, J.G., Schlez, W., Phillips, J., Rados, K., Zervos, A., Politis, E.S., and Chaviaropoulos, P.K.: Modelling and measuring flow and wind turbine wakes in large wind farms offshore, Wind Energy, 12(5), 431–444, doi:10.1002/we.348, 2009.

Bartl, J., Pierella, F., and Sætran, L.: Wake Measurements behind an Array of Two Model Wind Turbines, Energy Procedia,
5   24, 305-312, doi:10.1016/j.egypro.2012.06.113, 2012.

Bartl, J., and Sætran, L.: Experimental testing of axial induction based control strategies for wake control and wind farm optimization, paper accepted to The Science of Making Torque from Wind conference, to be published in Journal of Physics: Conference Series, 2016.

Benedict, L., and Gould, R.: Towards better uncertainty estimates for turbulence statistics, Experiments in Fluids, 22, 129–
10   136, doi:10.1007/s003480050030, 1996.

Crespo, A., Hernandez, J., Fraga, E., and Andreu, C.: Experimental validation of the UPM computer code to calculate wind turbine wakes and comparison with other models, Journal of Wind Engineering and Industrial Aerodynamics, 27(1–3), 77-88, doi:10.1016/0167-6105(88)90025-6, 1988.

Drela, M.: Xfoil 6.99, http://web.mit.edu/drela/Public/web/xfoil/, 2013.

15 Eriksen, P.E.: Rotor wake turbulence – An experimental study of a wind turbine wake, Doctoral thesis at NTNU, 2016:34, ISBN 978-82-326-1408-0, 2016.

Frandsen, S., Barthelmie, R., Pryor, S., Rathmann, O., Larsen, S., Højstrup, J., and Thøgersen, M.: Analytical modelling of wind speed deficit in large offshore wind farms, Wind Energy, 9 (1-2), 39–53, doi:10.1002/we.189, 2006.

Hallanger, A., and Sand, I.Ø.: CFD Wake modelling with a BEM wind turbine sub-model, Modeling, Identification and
20   Control, 34, 19–33, ISSN 1890–1328, 2013.

Hsu, S.A., Meindl, E.A., and Gilhousen, D.B.: Determining the power-law wind-profile exponent under near-neutral stability conditions at sea, Journal of Applied Meteorology, 33(6), 757-765, doi:10.1175/1520-0450(1994)033, 1994.

Jensen, N.O.: A note on wind generator interaction, Technical Report, Risø, RISØ-M-2411, orbit.dtu.dk/fedora/objects/orbit:88807, 1983.

25 Kocer, G., Mansour, M., Chokani. N., Abhari, R.S., and Müller, M.: Full-Scale Wind Turbine Near-Wake Measurements Using an Instrumented Uninhabited Aerial Vehicle, Journal of Solar Energy Eng., 133(4), doi:10.1115/1.4004707, 2011.

Kumer, V.M., Reuder, J., Svardal, B., Sætre, C., and Eecen, P.: Characterisation of Single Wind Turbine Wakes with Static and Scanning WINTWEX-W LiDAR Data, Energy Procedia, 80, 245-254, doi:10.1016/j.egypro.2015.11.428, 2015.

Krogstad, P.Å., and Eriksen, P.E.: 'Blind test' calculations of the performance and wake development for a model wind
30   turbine, Renewable Energy, 50, 325–333, doi:10.1016/j.renene.2012.06.044, 2013.

Krogstad, P.Å., Sætran, L., and Adaramola, M.S.: Blind Test 3 calculations of the performance and wake development behind two in-line and offset model wind turbines, Journal of Fluids and Structures, 52, 65–80, doi:10.1016/j.jfluidstructs.2014.10.002, 2015.

Larsen, G.C., Madsen, H.A., Larsen, T.J., and Troldborg, N.: Wake modeling and simulation, Technical Report, Risø-R-1653(EN), orbit.dtu.dk/fedora/objects/orbit:80992, 2008.

Ning, S.A.: A simple solution method for the blade element momentum equations with guaranteed convergence, Wind Energy, 17, 1327–1345, doi: 10.1002/we.1636, 2014.

5 Maal, G.T.: Parameter study of electric power production in wind farms - experiments using two model scale wind turbines, Master's thesis NTNU, brage.bibsys.no/xmlui/handle/11250/2350000, 2014.

Medici, D., and Alfredsson, P.H.: Measurements on a Wind Turbine Wake: 3D Effects and Bluff Body Vortex Shedding, Wind Energy, 9, 219–236, doi:10.1002/we.156, 2006.

Mendonça, F., Baris, O., and Capon, G.: Simulation of Radial Compressor Aeroacoustics Using CFD, ASME Turbo Expo
10   2012, Turbine Technical Conference and Exposition, Copenhagen, Denmark, 8, 1823-1832, Paper No. GT2012-70028, doi:10.1115/GT2012-70028, 2012.

Ostovan, Y., Amiri, H., and Uzol, O.: Aerodynamic Characterization of NREL S826 Airfoil at Low Reynolds Numbers, RUZGEM Conference on Wind Energy Science and Technology, METU Ankara Campus, 2013.

Pierella, F., Krogstad, P.Å., and Sætran, L.: Blind Test 2 calculations for two in-line model wind turbines where the
15   downstream turbine operates at various rotational speeds, Renewable Energy, 70, 62–77, doi:10.1016/j.renene.2014.03.034, 2014.

Prydz, E., Huuse, Ø., Müller, B., Bartl, J., and Sætran, L.: Numerical Simulation of Flow around the NREL S826 Airfoil at Moderate Reynolds numbers Using Delayed Detached Eddy Simulation (DDES), Proceedings ICNAAM 2016, ICNAAM_2016_124, 2016.

20 Sagmo, K.F., Sætran, L., and Bartl, J.: Numerical simulations of the NREL S826 airfoil, paper accepted to The Science of Making Torque from Wind 2016 conference, to be published in Journal of Physics: Conference Series, 2016.

Sanderse, B., van der Pijl, S.P., and Koren, B.: Review of computational fluid dynamics for wind turbine wake aerodynamics, Wind Energy, 14(7), 799–819, doi:10.1002/we.458, 2011.

Sarmast, S., and Mikkelsen, R.: The experimental results of the NREL S826 airfoil at low Reynolds numbers, Technical
25   Report, urn:nbn:se:kth:diva-120583, 2013.

Sarmast, S., Dadfar, R., Mikkelsen, R.F., Schlatter, P., Ivanell, S., Sørensen, J.N., and Henningson, D.S.: Mutual inductance instability of the tip vortices behind a wind turbine, Journal of Fluid Mechanics, 755, 705-731doi:dx.doi.org/10.1017/jfm.2014.326, 2014.

Schepers, J.G., Boorsma, K., and Snel, H.: IEA Task 29 MexNext: analysis of wind tunnel measurements from the EU
30   project Mexico, Proceedings of The Science of Making Torque from Wind, 169–178, 2010.

Schepers, J.G., Boorsma, K., and Munduate, X.: Final Results from Mexnext-I: Analysis of detailed aerodynamic measurements on a 4.5 m diameter rotor placed in the large German Dutch Wind Tunnel DNW, Journal of Physics: Conference Series, 555, doi:10.1088/1742-6596/555/1/012089, 2014.

Schümann, H., Pierella, F., and Sætran, L.: Experimental Investigation of Wind Turbine Wakes in the Wind Tunnel, Energy Procedia, 35, 285-296, doi:10.1016/j.egypro.2013.07.181, 2013.

Somers, D.M.: The S825 and S826 Airfoils, Technical Report NREL/SR-500-36344, wind.nrel.gov/airfoils/Documents/S825,S826_Design.pdf, 2005.

5 Sætran, L., and Bartl, J.: Invitation to the 2015 'Blind test 4' Workshop, Technical document NTNU, www.sintef.no/globalassets/project/nowitech/events/bt4_invitation2015.pdf, 2015.

Sørensen, J.N., and Shen, W.Z.: Numerical modeling of wind turbine wakes, Journal of Fluid Engineering, 124, 393-399, doi:10.1115/1.1471361, 2002.

Talmon, A.M.: The wake of a horizontal-axis wind turbine model, measurements in uniform inflow and in a simulated
10 atmospheric boundary layer, TNO Data report, publications.tno.nl/publication/100176/YosHZP/85-010121.pdf, 1985.

Trujillo, J.J., Seifert, J.K., Würth, I., Schlipf, D., and Kühn, M.: Full-field assessment of wind turbine near-wake deviation in relation to yaw misalignment, Wind Energy Science, 1, 41–53, doi:10.5194/wes-1-41-2016, 2016.

Van Leer, B: Towards the ultimate conservative differencing scheme II: Monotonicity and conservation combined in a second–order scheme, Journal of Computational Physics, 14, 361-370, 1974.

15 Wagner, R., Cañadillas, B., Clifton, A., Feeney, S., Nygaard, N., Poodt, M., St. Martin, C., Tüxen, E., and Wagenaar, J.W.: Rotor equivalent wind speed for power curve measurement – comparative exercise for IEA Wind Annex 32, Journal of Physics: Conference Series 524, 012108, doi:10.1088/1742-6596/524/1/012108, 2014.

Wheeler, A.J., and Ganji, A.R.: Introduction to engineering experimentation, Third edition, Upper Saddle River NJ, Pearson/Prentice Hall, XI, ISBN-13: 987-0-13-511314-1, 2004.

20

Table 1. Overview of turbine operating conditions, downstream turbine positions as well as wake measurement positions for the five different test cases.

Test case	Inflow	Inlet turbulence at position of T1	Tip speed ratio λ_{T1}	Position x/D of downstream turbine T2	Tip speed ratio λ_{T2}	Wake measurement position at x/D
A	uniform	0.23%	6.0	5.18	4.5	2.77
B1	uniform	10.0%	6.0	2.77	4.5	-
B2	uniform	10.0%	6.0	5.18	4.5	-
B3	uniform	10.0%	6.0	9.00	4.5	2.77 / 5.18 / 8.50
C	shear	10.1%	6.0	5.18	4.5	2.77

Table 2. Numerical values of power coefficient C_P and thrust coefficient C_T for test case A. The downstream turbine T2 is positioned at 5.18D downstream of T1. T1 is operated at λ_{T1}=6.0 and T2 is operated at λ_{T1}=4.5 referred to the far upstream reference velocity U_{ref}=11.5m/s.

		Upstream turbine T1		Downstream turbine T2	
		$C_{P,T1}$	$C_{T,T1}$	$C_{P,T2}$	$C_{T,T2}$
UU-DTU	▶	0.428	0.748	0.108	0.379
Vrije	◻	0.457	0.856	0.244	0.502
LUT (FRR)	◆	0.468	0.766	0.171	0.394
CD-adapco	★	0.470	0.820	0.170	0.460
CMR	◀	0.433	0.785	0.158	0.415
Experiment	●○	0.462	0.811	0.145	0.427

Table 3. Numerical values of power coefficient C_P and thrust coefficient C_T for test cases B_1, B_2 and B_3. The downstream turbine T2 is positioned at 2.77D (B_1), 5.18D (B_2) and 9.00D (B_3) downstream of T1. T1 is operated at λ_{T1}=6.0 and T2 is operated at λ_{T1}=4.5 referred to the reference velocity U_{ref}=11.5m/s.

		Upstream turbine T1		Downstream turbine T2 at 2.77D (B_1)		Downstream turbine T2 at 5.18D (B_2)		Downstream turbine T2 at 9.00D (B_3)	
		$C_{P,T1}$	$C_{T,T1}$	$C_{P,T2}$	$C_{T,T2}$	$C_{P,T2}$	$C_{T,T2}$	$C_{P,T2}$	$C_{T,T2}$
UU-DTU	▶	0.447	0.758	0.115	0.383	0.152	0.423	0.192	0.462
Vrije	■	0.453	0.853	0.115	0.336	0.149	0.415	0.166	0.486
LUT (ACL)	◆	0.453	0.788	0.157	0.449	0.228	0.518	0.339	0.605
LUT (FRR)	◆	0.456	0.756	-	-	0.194	0.419	-	-
CD-adapco	★	0.470	0.830	0.130	0.410	0.170	0.440	0.230	0.480
CMR	◀	0.436	0.785	0.145	0.411	0.218	0.490	0.294	0.576
Experiment	●○	0.468	0.833	0.137	0.423	0.188	0.500	0.270	0.569

Table 4. Numerical values of power coefficient C_P and thrust coefficient C_T for test case C. The downstream turbine T2 is positioned at 5.18D downstream of T1. T1 is operated at λ_{T1}=6.0 and T2 is operated at λ_{T1}=4.5 referred to the reference velocity U_{ref}=11.5m/s measured at hub height.

		Upstream turbine T1		Downstream turbine T2	
		$C_{P,T1}$	$C_{T,T1}$	$C_{P,T2}$	$C_{T,T2}$
UU-DTU	▶	0.432	0.745	0.139	0.405
LUT (FRR)	◆	0.451	0.758	0.197	0.426
CD-adapco	★	0.460	0.830	0.170	0.450
CMR	◀	0.431	0.782	0.182	0.452
Experiment	●○	0.453	0.785	0.184	0.486

Figure1. Model wind turbines (x/D=2.77) installed in the test section of NTNU's low speed wind tunnel.
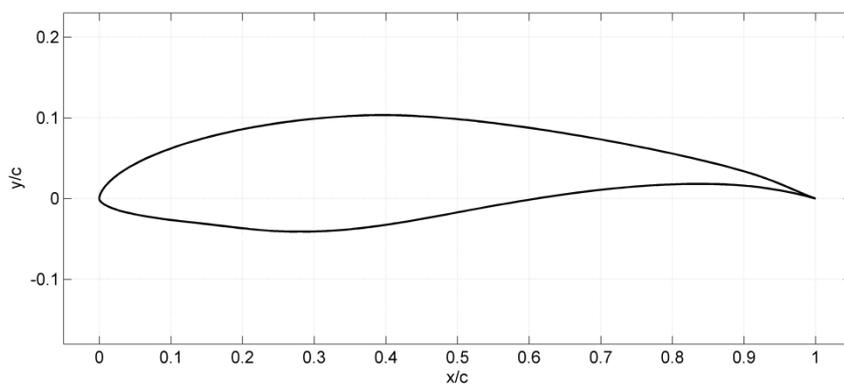
Figure 2. NREL S826 airfoil geometry.
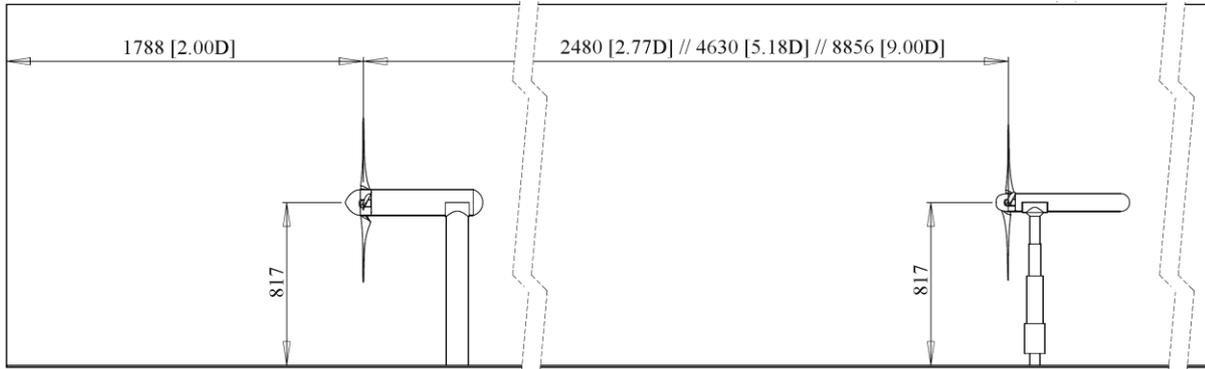
Figure 3. Setup of the model wind turbine in the wind tunnel.
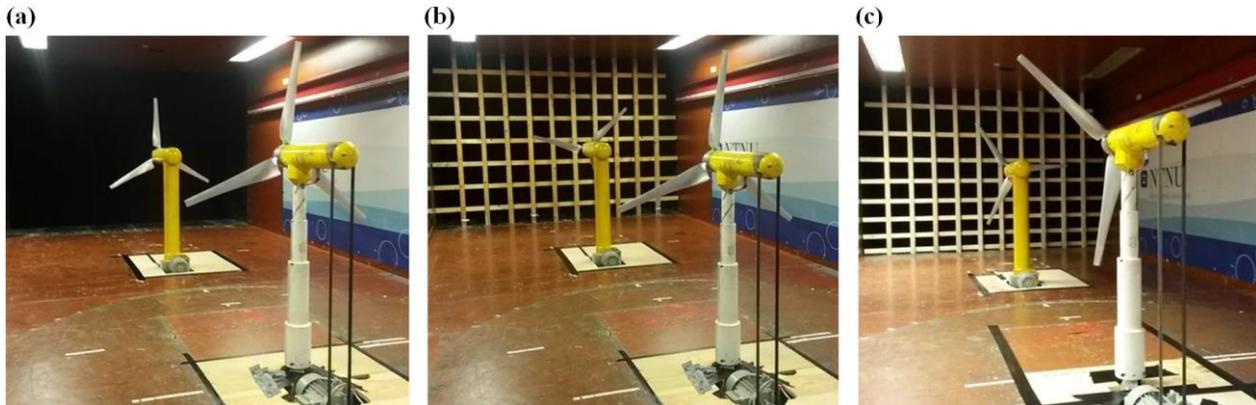
Figure 4. Test case A: low turbulence uniform inflow **(a)**; test case B: high turbulence uniform inflow **(b)**; test case C: high turbulence shear inflow **(c)**.

(a)

(b)
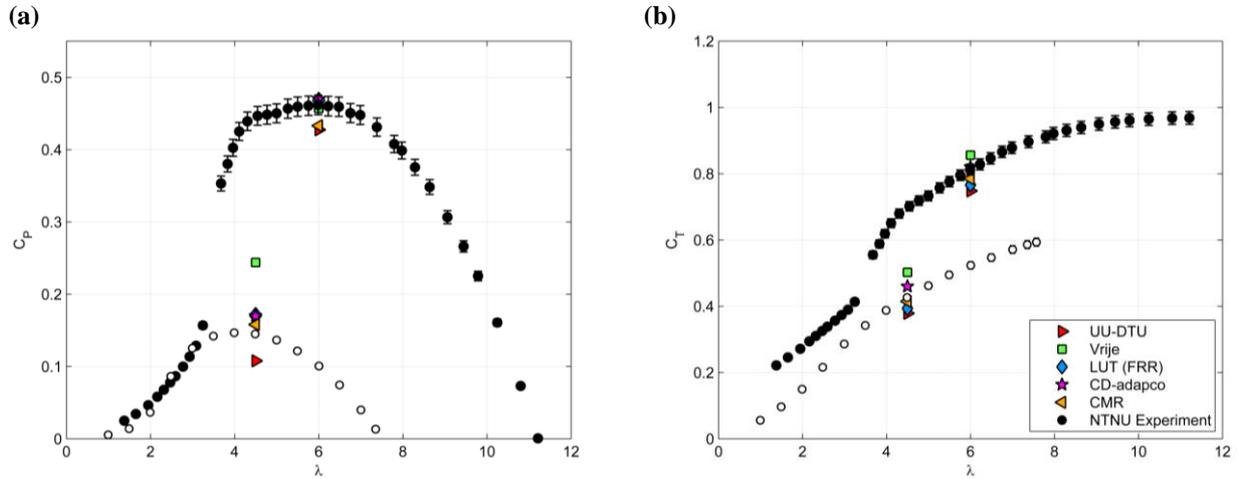
Figure 5. Power coefficient C_P **(a)** and Thrust coefficient C_T **(b)** for T1 (filled circles) and T2 (empty circles) compared for test case A. The downstream turbine T2 is positioned at x/D=5.18 downstream of T1 and the upstream turbine T1 is operated at λ_{T1}=6.0. The reference velocity is U_{ref} = 11.5m/s.

(a)

(b)

Figure 6. Normalized mean velocity U/U_{ref} **(a)** and normalized turbulent kinetic energy k/U_{ref} **(b)** in the wake x/D=2.77 behind T1 measured for test case A. The upstream turbine T1 is operated at λ_{T1}=6.0. The reference velocity is U_{ref} = 11.5m/s.

Figure 7. Power coefficient C_P **(a, c, e)** and Thrust coefficient C_T **(b, d, f)** for T1 (filled symbols) and T2 (empty circles) compared for test case B_1, B_2 and B_3. The downstream turbine T2 is positioned at x/D=2.77 **(a, b)**, 5.18 **(c, d)** and 9.00 **(e, f)** downstream of T1. The upstream turbine T1 is operated at λ_{T1}=6.0. The reference velocity is U_{ref} = 11.5m/s.

Figure 8. Normalized mean velocity U/U_{ref} **(a, c, e)** and normalized turbulent kinetic energy k/U^2_{ref} **(b, d, f)** in the wake $x/D=2.77$ **(a, b)**, 5.18 **(c, d)** and 8.50 **(e, f)** behind T1 for test case setup B_3. The upstream turbine T1 is operated at $\lambda_{T1}=6.0$. The reference velocity is $U_{ref} = 11.5$m/s.

WIND
ENERGY
SCIENCE
DISCUSSIONS
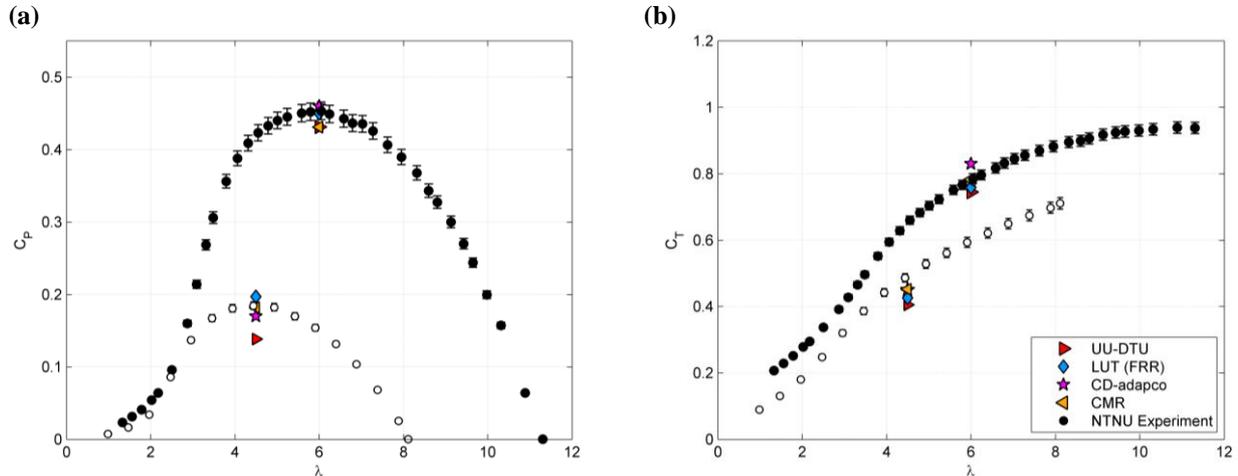
Figure 9. Power coefficient C_P **(a)** and Thrust coefficient C_T **(b)** for T1 (filled symbols) and T2 (empty circles) compared for test case C. The downstream turbine T2 is positioned at x/D=5.18 downstream of T1 and the upstream turbine T1 is operated at λ_{T1}=6.0. The reference velocity U_{ref} = 11.5m/s is the velocity experienced by T1 at hub height.
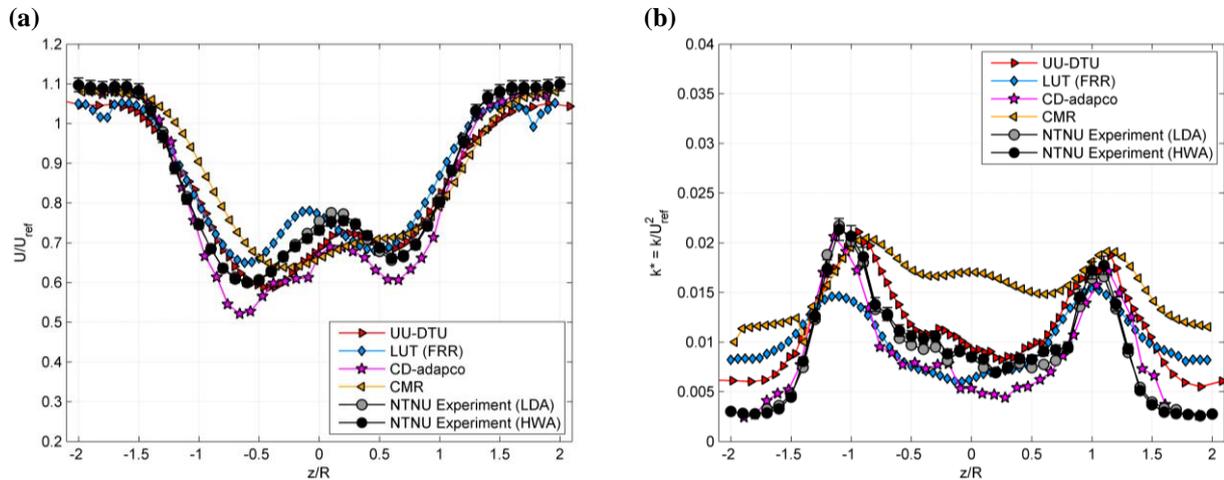
Figure 10. Normalized mean velocity U/U_{ref} **(a)** and normalized turbulent kinetic energy k/U_{ref} **(b)** in the wake x/D=2.77 behind T1 measured for test case C. The upstream turbine T1 is operated at λ_{T1}=6.0. The reference velocity U_{ref} = 11.5m/s is the velocity experienced by T1 at hub height.